

Characterization of CPC solar concentrators by a laser method

A. Parretta*^{1,2}, A. Antonini^{2,4}, M. Stefancich^{3,4}, V. Franceschini², G. Martinelli², M. Armani⁵

¹ENEA Centro Ricerche “E. Clementel”, Via Martiri di Monte Sole 4, 40129 Bologna (BO), Italy.

²Physics Department, University of Ferrara, Via Saragat 1, 44100 Ferrara (FE), Italy.

³CNR c/o Physics Department, University of Ferrara, Via Saragat 1, 44100 Ferrara (FE), Italy.

⁴CPower SRL Via Saragat 1, 44100 Ferrara (FE), Italy.

⁵Institute for Renewable Energy, EURAC research, Viale Druso 1, 39100 Bolzano (BZ), Italy.

*Phone: +39 (0)51 6098617; Fax: +39 (0)51 6098767; E-mail: antonio.parretta@bologna.enea.it

ABSTRACT

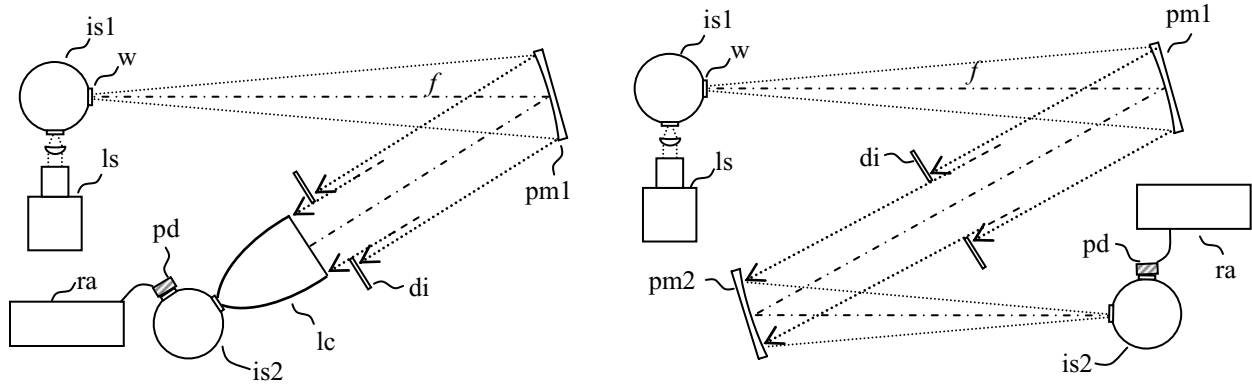
In this paper we present a method of optical characterization of solar concentrators based on the use of a laser beam. The method, even though constrained by lengthy measurements, gives nevertheless interesting information on local mirror surface defects or manufacturing defects, like internal wall shape inaccuracies. It was applied to 3D-CPC-like concentrators and the measurements were supported by optical simulations with commercial codes. The method, simple to apply, requires just a laser to scan the CPC input aperture following a matrix-like path, at a controlled orientation of the beam. Maps of optical efficiency as function of the laser beam incidence angle are obtained by matching the CPC exit aperture with a photodetector with an efficient light trapping. The integration of each map gives the CPC efficiency resolved in angle of incidence, so curves of optical transmission (efficiency) as function of incidence angle can be drawn and the acceptance angle measured. The analysis of the single maps allows to obtain interesting information on light collection by the different regions of CPC input area. It reveals, moreover, how the efficiency of light collection depends on several factors like surface reflectivity, number of reflections of the single beam, local angle of incidence, local surface defects, and so on. By comparing the theoretical analysis with the experimental results, it is possible to emphasize the effects directly related to manufacturing defects.

Keywords (OCIS): Integrating spheres (120.3150); Optical inspection (120.4630); Solar energy (350.6050); Optical design of instruments (120.4570).

1. INTRODUCTION

PV concentrator systems using nonimaging primary optical elements are emerging as valid alternatives to conventional imaging systems using parabolic mirrors or Fresnel lenses¹⁻³. In particular, concentrators of the 3D-CPC family (ref. [4] chapt. 4), when suitably modified to shorten their length and model the input aperture for the efficient packing in a module, show several potential advantages: low optical losses, high concentration levels, less sensitivity to sun misalignment. The optical characterization of a CPC concentrator can be performed by producing a collimated beam of solar divergence ($\sim 0.27^\circ$) impinging on the input aperture at different incidence angles with respect to the optical axis, and by measuring the flux collected at the exit aperture. The optical efficiency curve of the concentrator is in this way obtained together with the characteristic acceptance angle, that is the angle at which the efficiency shows a defined drop, typically 50% (ref. [4] chapt. 4). The typical experimental setup adopted for measurement of the optical efficiency of a light concentrator is schematically reported in Fig. 1. The light source (ls) illuminates the integrating sphere (is1) which acts as a source of diffuse light with constant radiance at its exit aperture, the window (w) of diameter D_w . A portion of light emerging from the sphere is collected by the parabolic mirror (pm1), placed slightly off-axis with respect to window (w) and at a distance from it equal to the focal distance f . The mirror (pm1) produces a parallel beam whose maximum angular divergence can be controlled by varying the diameter D_w . To obtain a beam with solar divergence ($\sim 0.27^\circ$) it is necessary to keep the ratio f / D_w equal to ~ 100 . The parallel beam, spatially filtered, is used to illuminate the solar concentrator (lc). The light at the exit aperture of concentrator (lc) is directed to

a second integrating sphere (is2) and its flux measured, through the photodetector (pd), placed inside (is2), by the radiometer (ra).

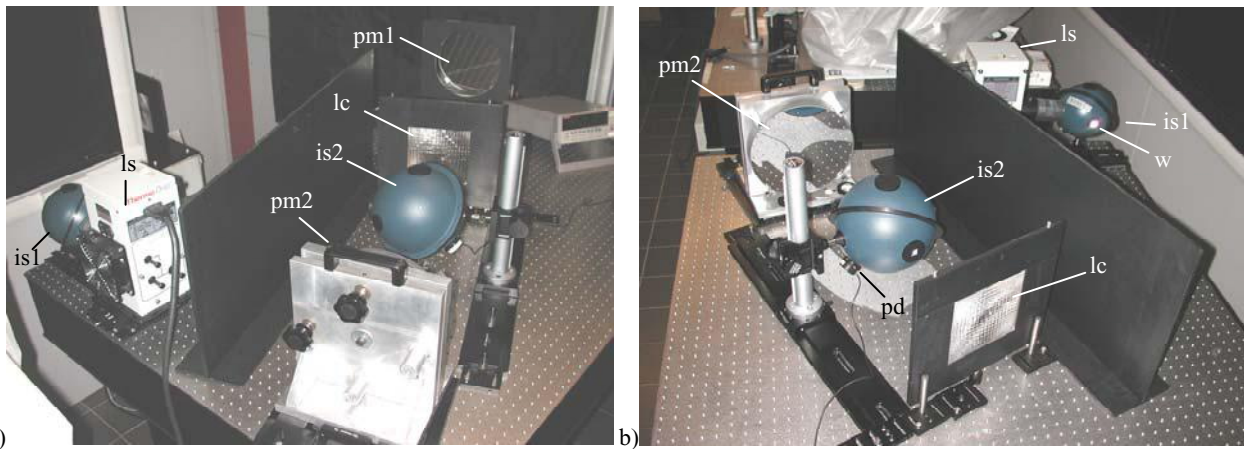


a) Schematic of the experimental setup used with the direct method for measuring the light collected by a solar concentrator (cpc) at different incidence angles. b) Reference setup used to measure the flux incident at input of the concentrator.

To perform the angle resolved measurements required to draw the optical efficiency curve, the concentrator (lc) is oriented with respect to the beam axis at different angles δ . To measure the absolute optical efficiency, also the incident flux at entrance of the concentrator must be measured. This can be made with a different experimental setup (see Fig. 1b) in which the (lc) of Fig. 1a is replaced with a second parabolic mirror (pm2) and the collimated beam focused on the same photodetector (pd). If the reflectivity R_{pm} of the second parabolic mirror is known, the angle resolved efficiency of the concentrator becomes:

$$\eta(\delta) = S_{CPC}(\delta) \cdot \frac{(1 - R_{pm})}{S_{ref}} \quad (1)$$

where $S_{CPC}(\delta)$ is the photodetector signal measured at different incidence angles δ with the setup of Fig. 1a and S_{ref} is the photodetector signal measured with the reference setup of Fig. 1b. Fig. 2 shows the photos of the experimental setup of Fig. 1a, applied to the characterization of a prismatic lens used in a photovoltaic system. The light source (ls) is an arc-Xe lamp illuminating the 6-inch diameter integrating sphere from Labsphere. The light from (pm1) is focused by lens (lc) into (is2), a 8-inch diameter integrating sphere from Labsphere. The signal from (pd) is sent to a voltmeter or a lock-in. In this second case the source light at output of (ls) or at output of (is1) must be modulated.



a) and b) Experimental setup of the direct method for measuring the light collected by the solar concentrator (lc) at different incidence angles. It is represented the measurement of efficiency of a prismatic lens used as primary solar concentrator. The reference setup is not shown.

To simulate the above experiment, we have used the TracePro[®] software for opto-mechanical modeling⁵ to raytrace an ideal (not truncated) 3D-CPC with $\delta_{acc}=5^\circ$ acceptance angle, 1-cm diameter exit aperture $2a'$ and different wall reflectivities R_w . The other dependent dimensional quantities are: 11.48-cm diameter input aperture $2a$, 71.3-cm length L and 132x geometric concentration ratio C_{geo} (ref. [4] chapt. 1). Fig. 3a shows two simulated optical efficiency curves obtained at $R_w = 1.0$ and 0.95 wall reflectivities. They are characterized by a quite flat response at low angles and a sharp drop at 50% in correspondence of the acceptance angle, as usual for any ideal CPC concentrator (ref. [4] chapt. 4).

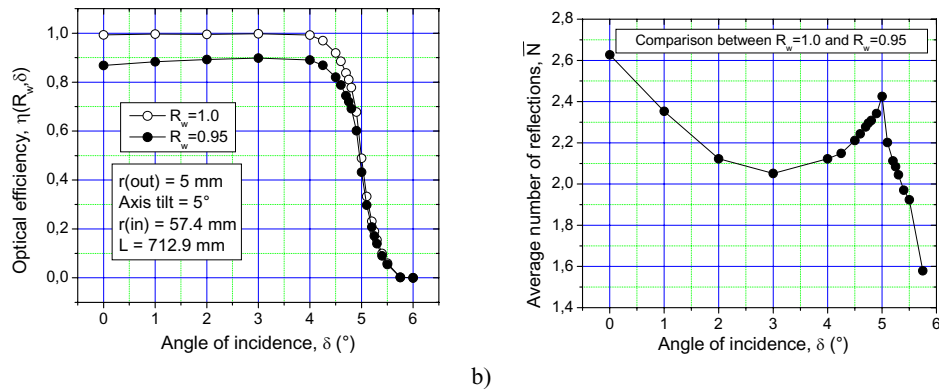


Figure 3. a) Absolute optical efficiency, or transmittance, curve obtained raytracing an ideal (not truncated) 3D-CPC concentrator with 5° acceptance angle, at two wall reflectivities (1.0 and 0.95). b) Average number of reflections onto the CPC internal wall of rays collected at the exit aperture.

A comparison between at least two efficiency curves, calculated for different wall reflectivities, R_w and R'_w , can be used to derive the average number of reflections the collected rays make onto the CPC wall. If Φ_{in} the constant input flux of a parallel beam (plane wave) incident at angle δ , and $\Phi_{out}(R_w, \delta)$ the generic flux available at output of the CPC with wall reflectivity R_w , the corresponding optical efficiency can be, indeed, expressed as:

$$\eta(R_w, \delta) = \Phi_{out}(R_w, \delta) / \Phi_{in} = \Phi_{out}(1.0, \delta) \cdot R_w^{\bar{N}(\delta)} / \Phi_{in} \quad (2)$$

from which the general formula for the average number of reflections becomes:

$$\bar{N}(\delta) = \ln \left[\frac{\eta(R_w, \delta)}{\eta(R'_w, \delta)} \right] / \ln \left[\frac{R_w}{R'_w} \right] \quad (3)$$

The quantity $\bar{N}(\delta)$, calculated by using the data of efficiency at $R_w = 1.0$ and $R'_w = 0.95$, is plotted in Fig. 3b. In the first part of the $\bar{N}(\delta)$ curve ($0 \leq \delta < \delta_{acc}$), where the number of output rays is almost constant, the efficiency is influenced by the number of reflections, and $\bar{N}(\delta)$ follows a trend opposite to that visible in the $\eta(0.95, \delta)$ curve of Fig. 2a. At δ_{acc} angle $\bar{N}(\delta)$ shows a relative maximum, and after that value the efficiency decreases mainly because of the loss of collected rays, even though $\bar{N}(\delta)$ is decreasing.

In this paper we introduce another “direct” method of characterization, different to that described in Fig. 1 in that it uses a laser as light source. By a simple laser beam we are able to investigate local areas of the concentrator and to reveal punctual defects, as mirror or substrate discontinuities, or more extensive defects, such as manufacturing inaccuracies. They in fact are able to affect both the intensity and the exit angle of the laser beam at the receiver aperture. Moreover, to distinguish between the effects introduced by surface defects and those caused by multiple reflections on the beam output flux, we compare the experimental results with simulations made on an optical model

of the concentrator with ideal surface optical properties. By these simulations we calculate the intensity and the exit angle of the laser beam at the receiver aperture.

2. EXPERIMENTAL

The “laser method” has been applied to the study of the optical properties of a 3D-CPC prototype, a truncated and squared CPC (TS-CPC), to be used as primary concentrator in a solar photovoltaic system. The prototype is derived from an ideal 3D-CPC, which has been truncated to reduce its length and its input aperture, originally of 14.3-cm diameter, has been squared to have the highest packing efficiency when assembling the units in a CPV module. The TS-CPC has an actual squared input aperture of 10-cm side, a circular output aperture of 1-cm diameter and a 35-cm length. The prototype has been realized by hollowing out a medium density polyurethane prism⁶, dividing it in two parts, and coating the internal walls by the VM2002 Radiant Mirror Film of 3M⁷. The coating of the internal wall was made provisionally by manually cutting thin strips of the film and sticking them on the wall surface. We expect therefore sensible optical effects from the deformation of the original substrate surface slope due to overlapping of adjacent strips. Fig. 4a shows the skeleton of the truncated and squared 3D-CPC (TS-CPC). Fig. 4b shows the TS-CPC prototype during a laser characterization. The specular reflectance of the TS-CPC wall was evaluated at $\lambda = 633$ nm for a randomly polarized beam by laser measurements at different incidence angles on a 3M film/substrate sample (see Fig. 5a). The reflectance resulted quite insensitive to incidence angle and the average value was 95 ± 1 %. The laser beam is used to scan the input aperture of the TS-CPC following a matrix-like path, at a well controlled orientation of the beam respect to the CPC optical axis (z axis).

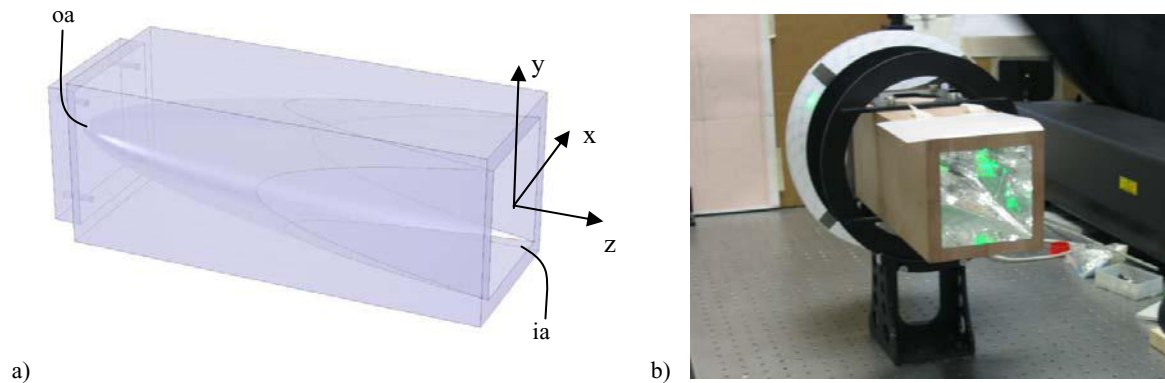


Figure 4. a) Perspective view of the truncated and squared 3D-CPC (TS-CPC) model used for simulation experiments with the laser method. The squared input aperture is (ia); the circular output aperture is (oa). b) The realized prototype of TS-CPC during a characterization by laser beam in laboratory.

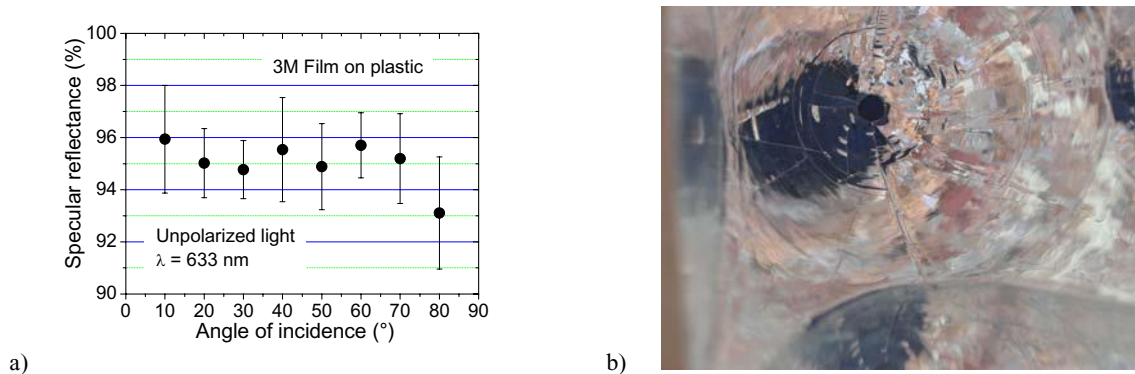


Figure 5. a) Data of specular reflectance of the 3M film/substrate sample at $\lambda = 633$ nm as function of the incidence angle of the laser beam. The average reflectance is 95 ± 1 %. b) Photo of the internal wall of the TS-CPC. It is visible the output aperture closed with the SPHECO252 cell.

Even though constrained by lengthy measurements, the laser method nevertheless showed to be very suitable to reveal information on local defects of mirror surface or manufacturing defects of the prototype. The experimental measurements have been supported by optical simulations with the TracePro[®] software for opto-mechanical modeling⁵.

3. THE BASIC LASER METHOD

Fig. 6a shows the schematic experimental setup of the “laser method” and Fig. 6b a photo of the simplest apparatus with a manually driven laser. The laser was a He-Ne laser 05-LHP321 from Melles Griot with $\lambda=633$ nm wavelength and 5 mW power.

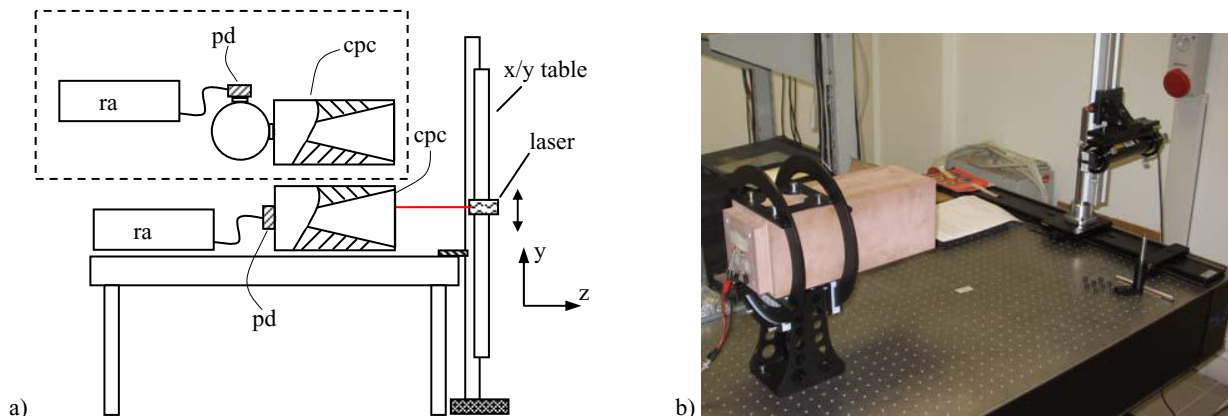


Figure 6. a) Schematic experimental setup of the “laser method”. The output flux can be measured directly by a photodetector (pd) or through an integrating sphere (see box). b) Photo of the apparatus with the manually driven laser.

The TS-CPC is positioned on a rotating support, provided with a goniometric scale, by which it is possible to fix the azimuthal angle of incidence of the laser beam. The incidence angle is adjusted by first aligning the laser beam with the TS-CPC, then projecting the beam on a far screen for adjusting the desired incidence angle. For an electronically driven movement of the source, the laser is fixed on the x/y table and moved following a matrix-like pattern of points, typically 25x25 points with 4 mm steps (see Fig. 6a). In a simpler setup the laser is moved manually along the vertical (y) direction on a column, and translated horizontally along x direction on a rail (see Fig. 6b). In this way the square aperture of the concentrator is entirely scanned along x and y directions.

3.1 Optical efficiency measurements

The light collected at output of the CPC is measured by a silicon photodetector (pd), the back contacts concentrating cell HECO252 of SunPower, controlled by the Kethley 199 System DMM / Scanner. The reference flux at input is obtained by a calibration step performed sending the laser beam directly on the (pd) surface. The map of (pd) signals is then transformed in a map of optical efficiency of the CPC by the ratio between test signals and average reference signal. The photodetector (pd) plays an important role in the precision of efficiency data. Its response in fact must be as much as possible insensitive to variations of incidence angle of laser beam at the exit aperture of the concentrator. With regard to this, the results of previous investigations on the angle-resolved absorbance of photovoltaic devices have been considered⁸. A preferred way to measure the flux at output of the CPC is to match it to an integrating sphere provided with a photodetector (pd) inside it (see Fig. 6a box).

Fig. 7 shows a series of experimental optical efficiency maps obtained at $\alpha = 0^\circ$ azimuthal angle (one edge of input aperture horizontal, see Figs. 4a, b), orienting the laser beam towards left (when looking at the CPC input aperture), at different incidence angles δ with respect to the z optical axis (see Fig. 4a). Besides the data of local absolute efficiency, each map brings also information about average efficiency and standard deviation. The summary of all the experimental data for efficiency of the total aperture, left side aperture and right side aperture, is reported in Table 1.

Fig. 8 shows, for comparison purposes, the efficiency maps simulated by TracePro™ for three significant angles of incidence: 0°, 1.5°, 2.5°. A look at the maps of Fig. 7 and 8 immediately gives plenty of information. First of all it is clear from $\delta = 0^\circ$ maps (Figs. 7a, 8a) that the real TS-CPC is not perfectly homogeneous as it should be. The right side of the experimental map is in fact slightly more efficient than left side, meaning that the right side mirror has been realized better. We note also a central region map considerably inefficient. This is due to a wrong mechanical shaping of the prism surface near the bottom of the CPC, and also to a more pronounced overlapping of film strips near to exit aperture. In the experimental $\delta = 0^\circ$ map it is also well visible the effect of joining the two portions of the prism by the less efficient vertical row at the center of the CPC. Another remarkable result is the average efficiency of the real TS-CPC at $\delta = 0^\circ$: 78.9%, to be compared to the theoretical 94.9% efficiency calculated with the assumption of a 95% wall reflectivity (see Fig. 5a). The theoretical results give an average number of reflections of light rays inside the TS-CPC of about one, as the loss of flux at each reflection is 5% and $\sim 5\%$ is the total calculated loss. The real prototype show a real efficiency far smaller. This fact demonstrates the unsuitability of the manually surface coating process, in spite of the high reflectivity of 3M film. At increasing incidence angle, the development of optical maps is quite clear. Both left and right side of input aperture show a decreasing efficiency. The more remarkable loss of efficiency on the left side is explained by the fact that at increasing incidence angles on the (ia) from right to left, the angle of impact of rays on the left side wall decreases (with respect to normal direction), with the consequent increase of the rejection probability for the rays.

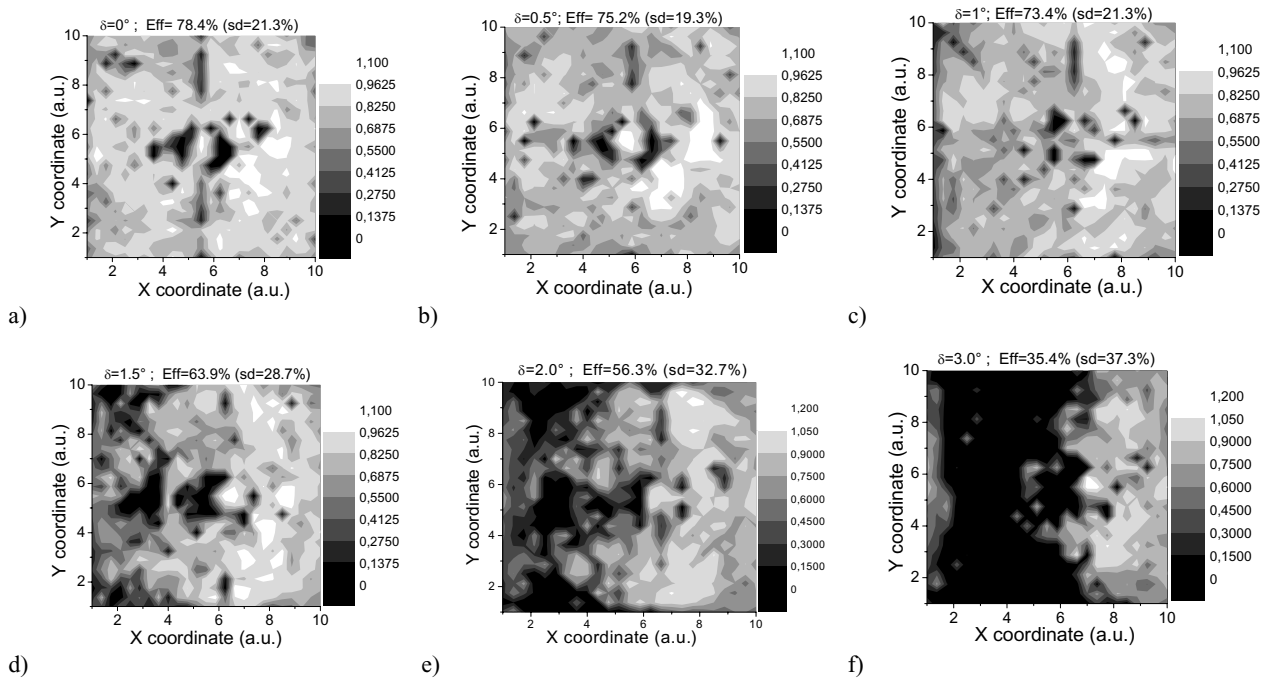


Figure 7. Experimental optical efficiency maps of the TS-CPC concentrator, obtained with the “laser method”. Azimuthal angle: $\alpha = 0^\circ$. Incidence angle: a) $\delta = 0^\circ$; b) $\delta = 0.5^\circ$; c) $\delta = 1.0^\circ$; d) $\delta = 1.5^\circ$; e) $\delta = 2.0^\circ$; f) $\delta = 3.0^\circ$.

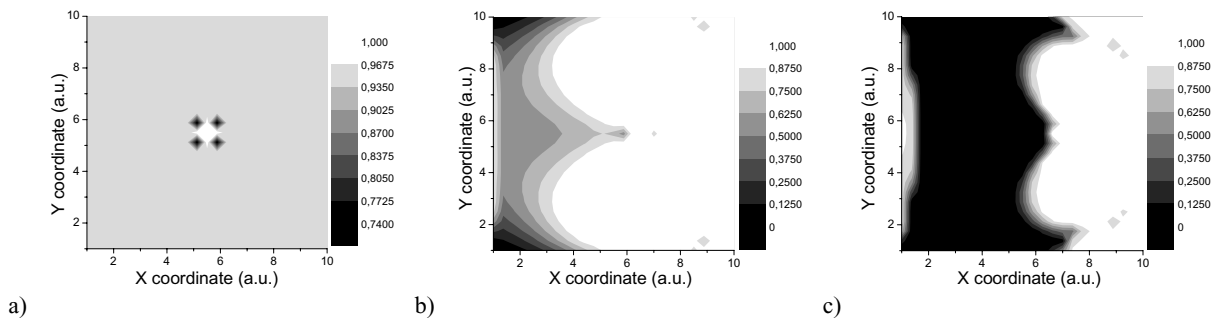


Figure 8. Simulated optical efficiency maps of the TS-CPC concentrator for the “laser method”. Azimuthal angle: $\alpha = 0^\circ$. Incidence angle: a) $\delta = 0^\circ$; b) $\delta = 1.5^\circ$; c) $\delta = 2.5^\circ$.

$\alpha(^{\circ})$	$\delta(^{\circ})$	Eff (%)	sd (%)	Eff (%) (left)	sd (%) (left)	Eff (%) (right)	sd (%) (right)
0	0	78.4	21.3	75.6	20.5	81.0	21.7
0	0.5	75.2	19.3	71.8	18.3	78.5	19.6
0	1.0	73.4	21.3	68.0	20.5	78.9	20.9
0	1.5	63.9	28.7	49.9	28.1	78.1	21.2
0	2.0	56.3	32.7	55.6	33.3	57.1	32.1
0	3.0	35.4	37.3	11.7	21.4	59.0	35.2
0	4.0	25.3	32.8	12.5	22.4	38.2	36.3
45	0	75.8	23.1	74.9	20.8	76.8	25.3
45	1.0	72.9	27.6	67.8	27.4	78.1	26.9
45	2.0	45.7	39.2	19.8	25.7	71.8	32.6
45	3.0	29.9	36.7	9.5	17.2	50.3	39.5
45	4.0	22.3	33.3	8.6	16.6	36.1	39.7

Table 1. Experimental efficiency data of the TS-CPC, obtained with the “laser method” at $\alpha = 0^{\circ}$ and 45° azimuthal angles.

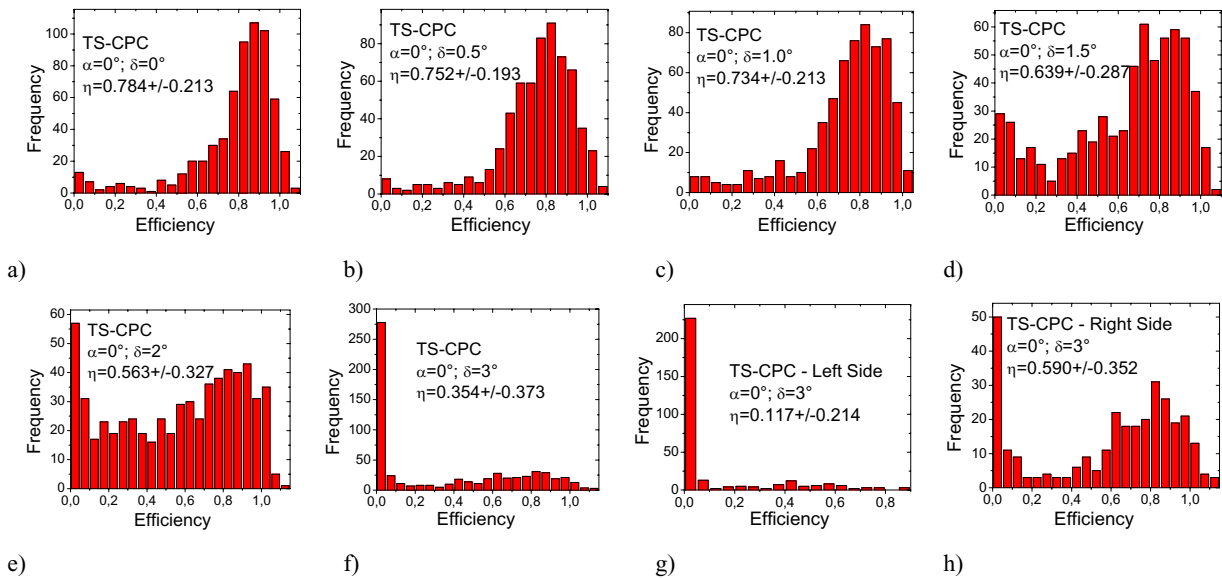
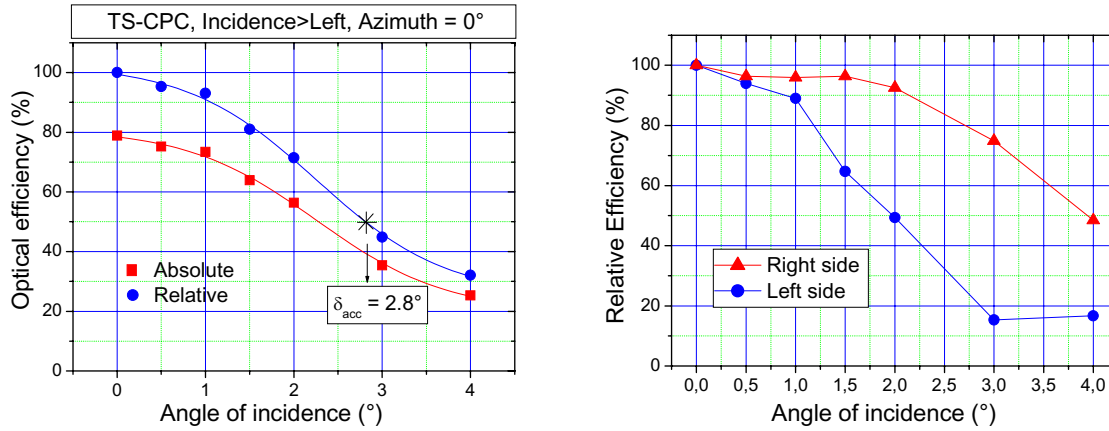


Figure 9. a-f) Frequency distribution of optical efficiency of TS-CPC in the different maps of Fig. 7. Azimuthal angle: $\alpha = 0^{\circ}$. Incidence angle: a) $\delta = 0^{\circ}$; b) $\delta = 0.5^{\circ}$; c) $\delta = 1.0^{\circ}$; d) $\delta = 1.5^{\circ}$; e) $\delta = 2.0^{\circ}$; f) $\delta = 3.0^{\circ}$. g, h) It is shown the frequency distribution at $\delta = 3.0^{\circ}$ separately for the left and right side of aperture window, respectively.

At $\delta = 2\div 3^{\circ}$ incidence, the loss of rays on left side aperture is remarkable, indicating that we are in the proximity of the acceptance angle (50% efficiency). In practice the left side is not efficient at all ($\eta < 15\%$). At 4° incidence a large part of input window, and then of CPC, is not efficient at all. Due to the strong difference found between left and right side efficiency, we have plotted separately the two efficiencies (see Fig. 10b). After 1° and up to 4° incidence, the two efficiency curves sensibly diverge. At $\delta = 3.0^{\circ}$, near the acceptance angle, there is the maximum difference between them (ratio of 0.2 between left side and right side) (see Fig. 11a). We note incidentally a sort of on/off optical switch behavior for light entering in the TS-CPC at $\sim 3^{\circ}$ incidence: “off” for light impinging on the left side, “on” for light impinging on the right side. This fact is well illustrated by the frequency graphs of Figs. 9g, h. The efficiency data of Table 1 give (see Fig. 10a) the angle-resolved optical efficiency curves, absolute $\eta(\delta)$ and relative $\eta_{rel}(\delta)$, of TS-CPC for $\alpha = 0^{\circ}$ azimuth and $\lambda = 633$ nm wavelength. From them we derive an acceptance angle of $\delta_{acc} = 2.8^{\circ}$ in correspondence of a 50% efficiency loss ($\delta_{acc} = 1.0^{\circ}$ in correspondence of a 10% efficiency loss). The experimental relative efficiency of the TS-CPC has been compared with other efficiencies calculated by using TracePro: one obtained simulating the “direct method”, the other simulating the “inverse method” (see Fig. 11b)⁹. The experimental efficiency is clearly affected by several factors: imperfections of TS-CPC wall shape; imperfections of 3M coating surface and loss of light by scattering; wall reflectivity of dependent on incident angle of impinging rays,

photodetector response dependent incidence angle of collected rays; laser characterization realized on a matrix of points of the input aperture (input aperture area not fully illuminated).



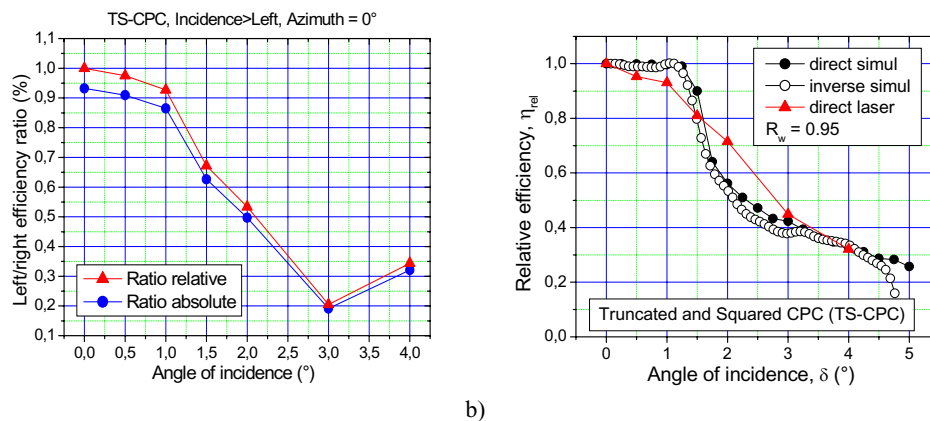
a) b)
Figure 10. Experimental optical efficiency curves of the TS-CPC concentrator for 0° azimuthal angle. a) Absolute and relative efficiency for the entire input aperture. b) Relative efficiency calculated separately for left side and right side input aperture.

Despite all these sources of errors, the experimental laser $\eta_{rel}(\delta)$ curve shows a not too much bad matching with the theoretical ones (acceptance angle $\delta_{acc} \sim 2.2^\circ$).

The optical efficiency of the TS-CPC has been measured also for 45° azimuth. Fig. 12 shows the efficiency maps calculated for the incidence angles: a) $\delta = 0^\circ$; b) $\delta = 1.0^\circ$; c) $\delta = 2.0^\circ$; d) $\delta = 3.0^\circ$; e) $\delta = 4.0^\circ$. The average value of efficiency and standard deviation for each incidence angle is reported in Table 1. From the angle-resolved efficiency we derive an acceptance angle: $\delta_{acc} \sim 2.3^\circ$ at 50% efficiency ($\delta_{acc} \sim 1.2^\circ$ at 90% efficiency), slightly lower than that measured at 0° azimuth.

3.2 Beam exit angle measurements

The measurement of exit angles of the laser beam collected at the output aperture has been carried out by using the simple apparatus illustrated in Fig. 12. A plastic hemispherical globe (hg) is centered on the output aperture of the TS-CPC and drawn with parallels and meridians to indicate the zenith and azimuth angles of the laser beam spot.



a) b)
Figure 11. a) Ratio between absolute (relative) efficiency of left side and right side of TS-CPC entrance window. b) Relative optical efficiency of the TS-CPC obtained by direct and inverse methods. The experimental efficiency curve (direct laser) is that obtained by characterizing the TS-CPC with the actual laser method. The other two curves have been obtained simulating the direct method and the inverse method⁹.

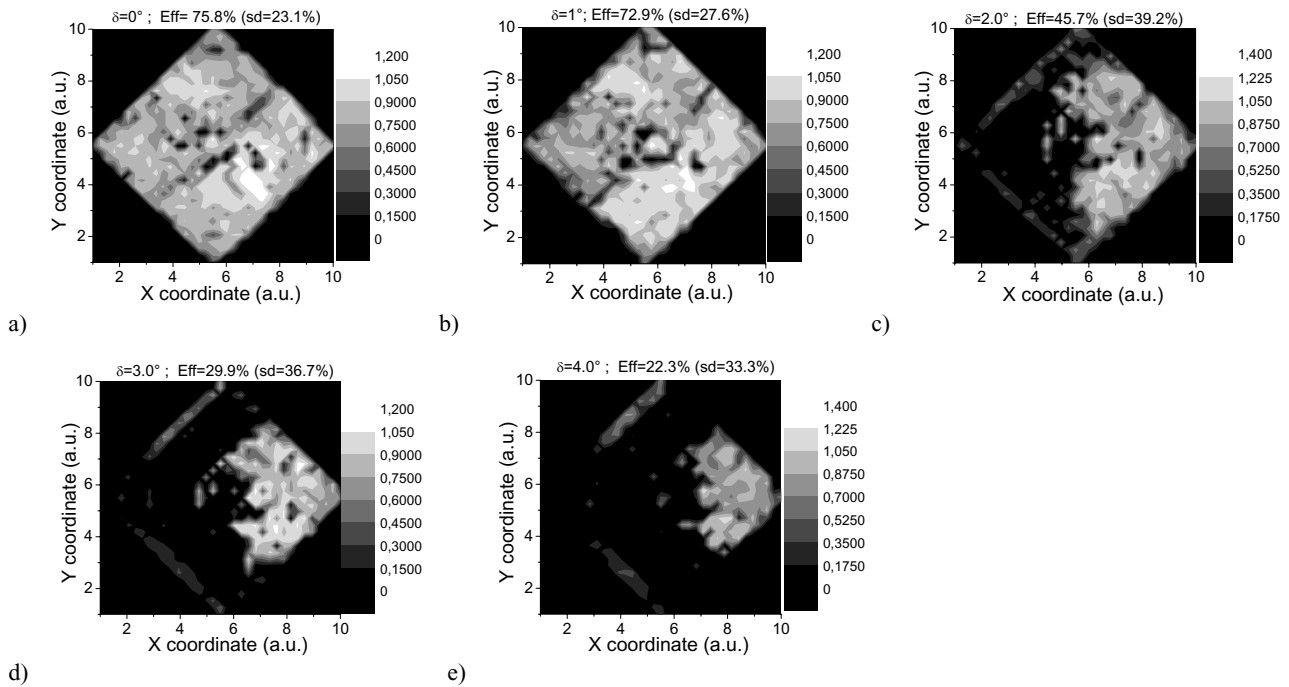


Figure 12. Experimental efficiency maps of TS-CPC concentrator, obtained with the “laser method”. Azimuthal angle: $\alpha = 45^\circ$. Incidence angle: a) $\delta = 0^\circ$; b) $\delta = 1.0^\circ$; c) $\delta = 2.0^\circ$; d) $\delta = 3.0^\circ$; e) $\delta = 4.0^\circ$.

The opalescence of the globe allows to visualize the impact point of the laser beam and then, with a good approximation, its exiting direction. Fig. 13a shows how the two exit angles are measured: the zenith angle ζ (0° - 90°) on the parallels and the azimuth angle α (0° - 360°) on meridians, where α is measured for rotation of y axis towards x axis. The lengthy manual measurements suggested us to draw only maps of azimuth and zenith angle at $\delta = 0^\circ$ incidence (laser beam parallel to the z optical axis) (see Fig. 14). Each point of the TS-CPC input aperture is represented by a value of the correspondent angle. The maps of Fig. 14 are very interesting for the beauty of the representation. Both have a well defined symmetry. The zenith angle map shows that rays incident on the periphery of input aperture (ia) exit from the TS-CPC with a small divergence. The divergence increases at decreasing the distance between impact point and center of (ia).

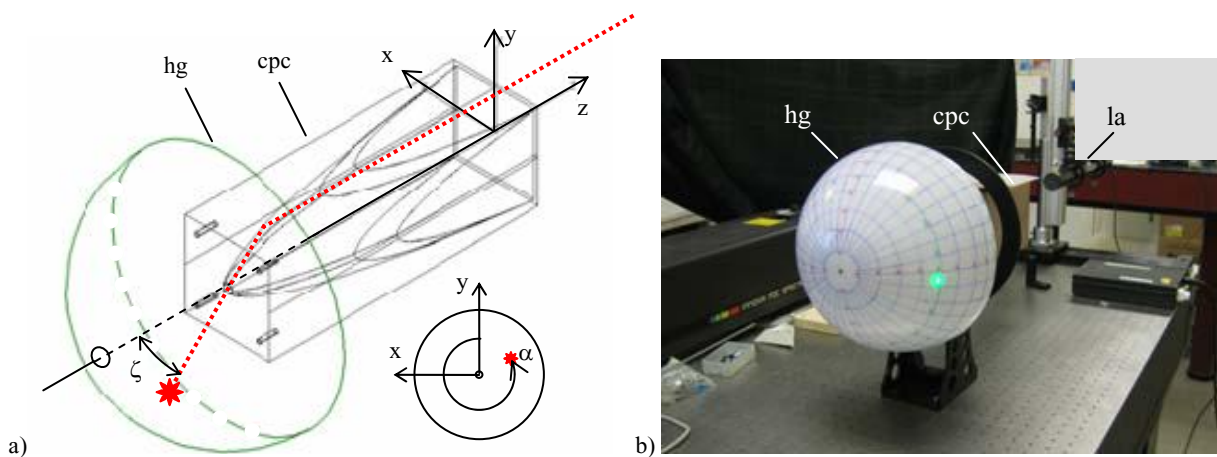


Figure 13. a) Schematic of the experimental configuration for measurement of beam exit angle. It is illustrated a ray entering into the TS-CPC and exiting at the zenithal angle ζ . The azimuthal angle is measured by rotating the y axis towards the x axis. b) Photo of the apparatus with the hemispherical globe (hg) fixed to the CPC and the laser.

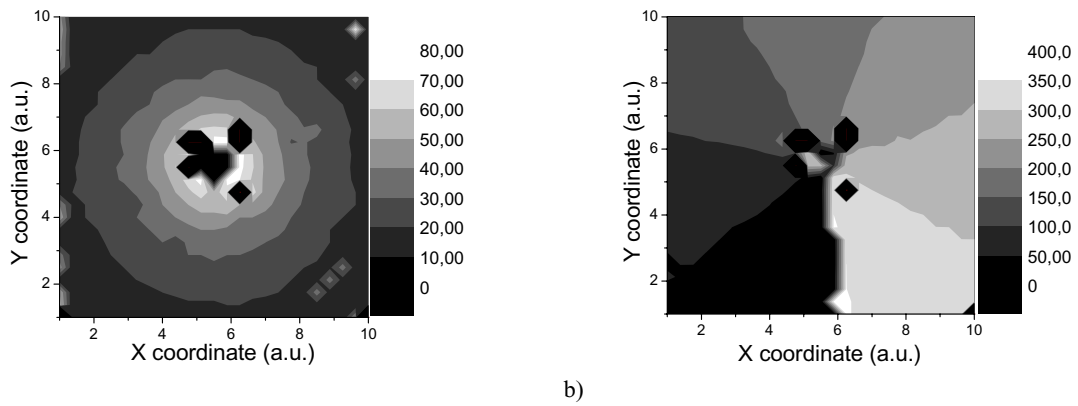


Figure 14. Input aperture maps of zenithal (a) and azimuthal (b) angles of the laser beam exiting from the TS-CPC, at $\delta = 0^\circ$.

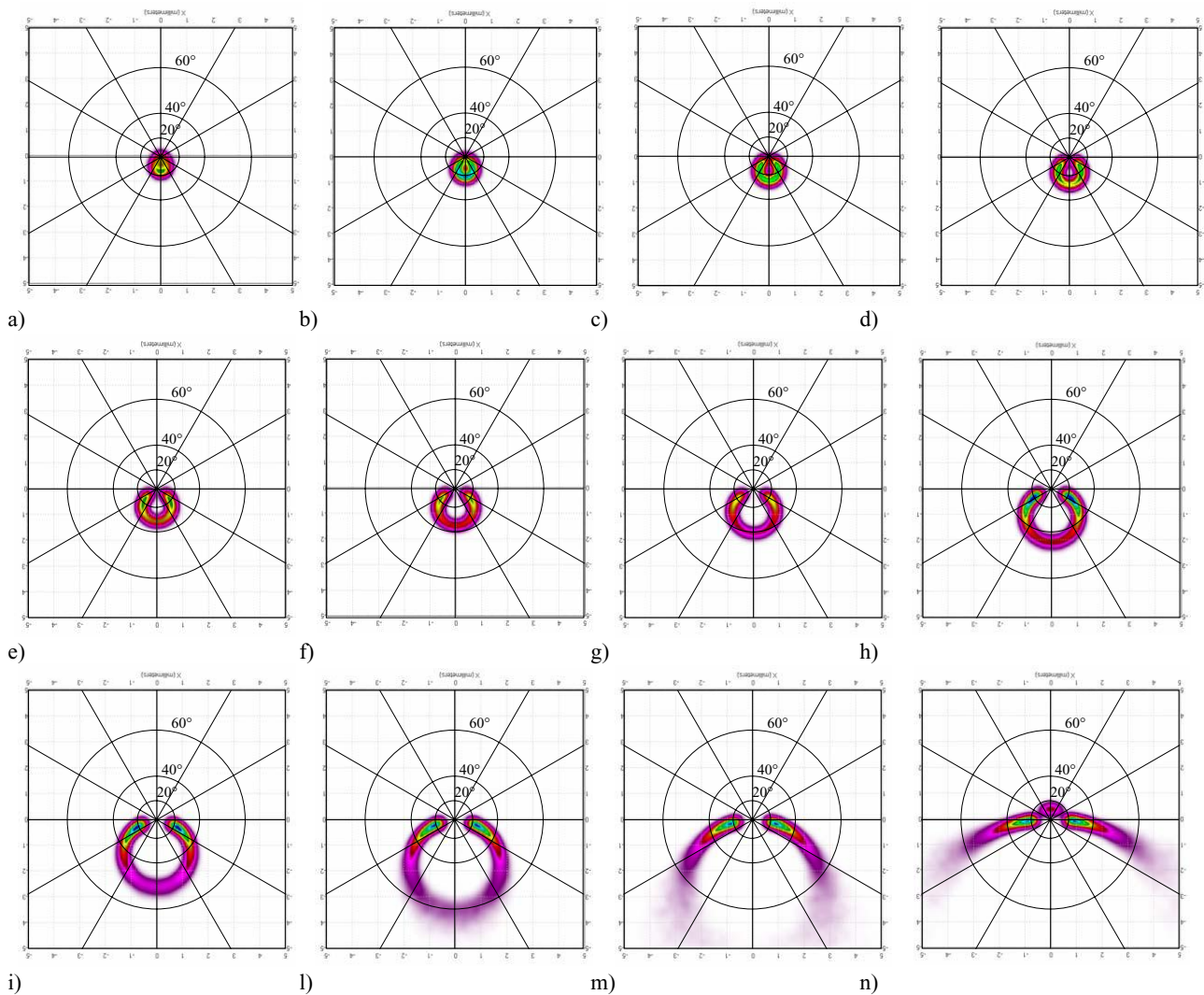


Figure 15. Optical path of exit beam as obtained scanning different horizontal lines on the input aperture of the TS-CPC and projecting the output beam on a 10-cm size planar screen, 2-cm far apart from the CPC.
a) $y = 4.8$ cm; b) $y = 4.4$ cm; c) $y = 4.0$ cm; d) $y = 3.6$ cm; e) $y = 3.2$ cm; f) $y = 2.8$ cm; g) $y = 2.4$ cm; h) $y = 2.0$ cm; i) $y = 1.6$ cm; l) $y = 1.2$ cm; m) $y = 0.8$ cm; n) $y = 0.4$ cm.

The regularity of this result is assured by the fact that the number of reflections is virtually one for any point of (ia), as results also by simulations with TracePro. The central region of zenith map is rather confused. Here the beam spot on the screen (hg) is strongly dispersed and so impossible to measure. The cause is the same affecting the efficiency maps at the central region (see Figs. 7 and 12): the wrong shaping of the prism surface near the bottom of CPC, and the pronounced overlapping of film strips near the exit aperture, which produce a strong scattering of the beam towards unpredictable directions. Fig. 14b shows that the azimuth angle also varies very regularly with the coordinate of input beam. It is possible to note that at an entrance point on (ia) corresponds an exit direction opposite with respect to the centre of aperture. Then, if we let the input ray move on a circle clockwise around the centre, the exiting azimuth will regularly increase and the zenith angle will remain constant. At the centre of the map we note the same irregularities as for the zenith angle map.

Another way of describing the change of direction of the exit beam is to draw its path on a planar screen as function of the y coordinate of a line scanned on the input aperture. An example is shown in Fig. 15, where horizontal lines are scanned, with steps of 4 mm, with a 1-mm diameter laser beam on the (ia) of the TS-CPC at different y coordinates, with steps of 4 mm. Only the upper half of TS-CPC has been explored, starting from $y = 4.8$ cm and going down to $y = 0.4$ cm. The path of exit beam is ring shaped, has an azimuthal excursion varying between $\pi/2$ and π depending on the y coordinate, and its maximum divergence (zenith) approaches progressively $\pi/2$ when the scanned line approaches the centre of input aperture.

4. CONCLUSIONS

The laser characterization of CPC concentrators, performed scanning the input aperture through a matrix of points, is a powerful method for revealing local defects of the internal reflecting wall and manufacturing inaccuracies of the substrate surface. The imperfections in the real concentrator were better revealed by comparing the optical measurements with simulations made on the CAD model of the prototype. In this paper we have analyzed in particular maps of local efficiency as function of orientation of the incident beam. Keeping the CPC exit aperture open, we have also studied the exit beam angular dependence as function of beam position on the input aperture.

We have characterized truncated and squared 3D-CPCs (TS-CPC) and derived the angle-resolved optical efficiency curves, both absolute and relative, and the associated acceptance angle. The effect of the CPC length shortening and input aperture square shaping determines a sensible rounding off of the efficiency curves, which for the corresponding ideal 3D-CPC is of the step type instead. Left and right sides of the TS-CPC input aperture show a strong difference in efficiency at near the acceptance angle.

The same laser method can be easily extended to the characterization of imaging concentrators (parabolic mirrors, Fresnel lenses).

ACKNOWLEDGMENTS

We acknowledge the support given by P. Colombani for the realization of the CPC concentrators.

REFERENCES

- [1] G. Martinelli, C. Malagù, M. Stefancich, D. Vincenzi, A. Parretta and R. Winston, "Optical beam splitting and CPC for high performances photovoltaic concentrator systems" oral presentation at the "19th Congress of International Commission for Optics, ICO XIX, Optics for the Quality of Life", Firenze, 25-30 August 2002. Technical Digest vol. II, ed. By A. Consortini and G.C. Righini (Washington, USA: SPIE Vol. 4829)2002, pp. 1023-1024.
- [2] A. Parretta, G. Martinelli, M. Stefancich, D. Vincenzi and R. Winston, "Modelling of CPC-based photovoltaic concentrator" oral presentation at the "19th Congress of International Commission for Optics, ICO XIX, Optics for the Quality of Life", Firenze, 25-30 August 2002. Technical Digest vol. II, ed. By A. Consortini and G.C. Righini (Washington, USA: SPIE Vol. 4829) 2002, pp. 1011-1012.
- [3] A. Parretta, M. Morvillo, C. Privato, G. Martinelli and R. Winston, "Modelling of 3D-CPCs for concentrating photovoltaic systems" oral presentation at the Conference "PV in Europe, from PV Technology to Energy

- Solutions”, Rome, Italy, 7-11 October 2002. Ed. J.L. Bal, G. Silvestrini, A. Grassi, W. Palz, R. Bigotti, M. Gamberane, P. Helm. WIP-Munich and ETA-Florence, 2002, pp. 547-550.
- [4] R. Winston, J.C. Miñano and P. Benítez, “*Nonimaging Optics*” Elsevier Academic Press, Burlington, MA 01803, USA, 2005.
 - [5] Lambda Research Corporation, 80 Taylor Street, P.O. Box 1400, Littleton, MA 01460, <http://www.lambdares.com/>.
 - [6] Paolo Colombani Design, Ferrara, Italy, www.paolocolumbani.com.
 - [7] www.3m.com/radiantlightfilm
 - [8] A. Parretta, A. Sarno, P. Tortora, H. Yakubu, P. Maddalena, J. Zhao, A. Wang, “Angle-dependent Reflectance and Transmittance Measurements on Photovoltaic Materials and Solar Cells”, *Optics Communications*, **172** (1999) 139-151.
 - [9] A. Parretta, A. Antonini, M. Stefancich, G. Martinelli, M. Armani, “Inverse illumination method for characterization of CPC concentrators”, oral presentation 6652-04 at this Conference, “Optical Modeling and Measurements for Solar Energy Systems”, Session 1, “Solar Energy Systems and Components” .